Article

Permeability Enhancement Induced by Fracture Shear Dilation During Close-Range Coal Seam Mining

Chao Li [1,2], Yingke Liu [1], Mingyao Wei [3,*] and Jinmiao Zhang [1]

1   School of Safety Engineering, China University of Mining and Technology, Xuzhou 221116, China
2   State Key Laboratory of Coal and CBM Co-Mining, Jincheng 048012, China
3   National Joint Engineering Laboratory of Internet Applied Technology of Mines, China University of Mining and Technology, Xuzhou 221116, China
*   Correspondence: cumtwmy@sina.com; Tel.: +86-51683590839

Abstract: The advance of the working face in coal seams alters the local stress field and may give rise to fractures in the vicinity of the excavation. In this study, a constitutive model in which damage is defined as a function of volumetric strain was established and utilized in a numerical model to prognosticate the fracture development around the excavation. The predicted fractures that emerged in the overlying rock mass were found to exhibit hybrid characteristics. A permeability model was also constructed, taking into account both tension- and shear-induced fracture development. The permeability increase of the upper adjacent coal seam is most notable within 40 m from the goaf boundary. As the working face progresses, the permeability of the upper adjacent coal seam is further enhanced while that of the lower adjacent coal seam remains unaffected. The permeability at the goaf boundary is high and reaches its maximum at the rear of the working face, indicating that for the permeability change, the effect of shear-induced dilation plays a more crucial role than that of pressure-dependent compaction. This study can be used to guide the design of coal seam methane drainage for the mining of closely spaced coal seams.

Keywords: coal mine goaf; gas drainage; permeability; adjacent coal seams; numerical simulation

1. Introduction

Currently, coal remains the main source of energy in China. However, with the increasing depth of coal mining, there is a risk of coal and gas outbursts in many coal seams. Moreover, the gas content and gas emission in coal seams are significantly high, severely restricting the safe and efficient mining of coal. Gas drainage is an important method to prevent gas disasters [1]. Most coal seams in China are mainly characterized by low permeability, and it is difficult to perform surface drilling or underground pre–drainage of the original coal gas [2]. Under the effect of mining, stress is relieved from the coal seams and the surrounding coal-rock strata, and the permeability significantly increases, sometimes reaching tens or even hundreds of times higher than the in situ values. Hence, the stress relief can significantly improve the subsequent gas drainage at the working face [3,4]. After coal seam mining, the goaf and the surrounding rock will generate an excavation-induced fracture zone that varies with the advance distance [5]. Methane migration and storage are closely related to the overburden fracture evolution and morphological variations. Therefore, it is of great significance to study the evolution of the overburden fracture and its permeability under the effect of mining to enhance the gas drainage effect and prevent gas outburst disasters [6–9].

Excavation in one zone is of great consequence in controlling the stability of adjacent coal seams. Additional coupling of the effects of stress, permeability, and desorption provides potential positive feedback to the liberation of gas. The evolution and distribution of mining-induced fractures during mining have been investigated, but their effects on the subsequent gas drainage remain to be studied [10,11]. Studies have established the

discriminant principles and methods for high-level annular fractured bodies using real-time monitoring and numerical simulation approaches [12–15]. Qian and Xu [16,17] studied the distribution characteristics of mining-induced fractures in overlying strata and put forward the O-shaped circle theory for mining-induced fractures. An O-shaped circle of the overburden was found to be an effective area for gas pressure relief drainage. Based on this, Lin et al. [8] proposed a simplified engineering model of mining-induced fractures with rounded corners and rectangular ladder belts, and analyzed the factors influencing the morphology of the mining-induced fracture zone.

During longwall mining, three different evolving zones exist in the overburden: A caving zone, a fracture zone, and a continuous deformation zone [18–20]. Huang et al. [21] proposed the method to determine the overburden fracture zone in the goaf based on the relevant mechanism. Yang and Xie [22] and Li et al. [23] found four evolving features of mining-induced fractures in the overburden from similarity simulation experiments: ∩–shaped cap, a hump shape low at the front and high at the back, a hump shape with equal levels from front to back, and a hump shape high at the front and low at the back. They proposed that the mining-induced fracture zone in the overburden does not exhibit a conventional layered distribution, but an ellipsoidal distribution when fracture and separation fissures are connected. Zhang et al. [24] monitored mining-induced fractures with a borehole color monitoring system and found that the fractures are mainly large-angle longitudinal cracks and that they gradually develop into fractures as the distance from the roof decreases. Cheng et al. [25] studied the pore-fracture evolution of coal under different confining pressures. The ultimate performance of CBM migration in mining-disturbed strata was determined. Tu and Liu [26] found that the main channel for methane migration is in the overburden fracture zone above the accumulation zone, based on the combined theory of methane migration and ground pressure. Karacan et al. [27] established a comprehensive dynamic reservoir model of a multichannel longwall wellsite and showed that the characteristics of gas production in coal seams and other gas-bearing strata are affected by subsidence. Lunarzewski [28] developed "Floor gas" and "Roof gas" simulation programs to characterize the stratigraphic relaxation zone, gas emission boundary, and gas emission prediction parameters. Additionally, Yu et al. [29] and Cheng and Yu [30] verified the stress relief antireflection effect of mining overburden based on engineering practice. Zhao et al. [31] analyzed the gas drainage performance in coal seams with different combinations of tectonically deformed sub-layers and intact sub-layers.

Therefore, understanding the coal seam disturbance by close-range mining and its effect on permeability is important in the context of coal seam gas drainage and management. Various studies have been conducted on the deformation and failure mechanisms of overlying rock mass and their contributions to the subsequent methane migration from coal seams. However, most of these studies are focused on a single coal seam, while the study for the case of mining a group of close-range coal seams need to be conducted. Mining coal seams has a considerable influence on the adjacent seams when they are close. On the one hand, the stress relief causes the redistribution of the local stress field and resultant deformation. It could also trigger the failure of the upper and lower adjacent coals and change their permeability significantly. On the other hand, the connection between the overburden fracture and adjacent coal seams causes gas emissions from the fracture field, affecting the gas distribution in the goaf. It has been demonstrated that neglecting the effect of shear dilation may lead to an underestimation of the coal permeability variation [32]. Specifically, shear dilation could enhance permeability by up to 2–3 orders of magnitude in the process of close-range coal seam mining, which is often ignored in previous research. In this paper, a permeability model under the competing influence of effective stress, shear deformation, and induced damage was proposed. Through theoretical analysis and numerical simulation, this study analyzed the permeability evolution process of the overburden space in coal mines and the law of mining-induced stress relief in adjacent coal seams during mining in close-distance coal seam groups, followed by an examination based on field test results.

2. Constitutive Model of Coal-Rock Mass

The coal-rock mass is a natural geological material with many types of joints, fissures, and micro-defects. However, the development and evolution of microcracks have an evident influence on the mechanical properties of materials, which can lead to damage to the materials themselves. In the mechanical sense of solid materials, damage refers to the generation and propagation of micropores or microcracks. To investigate the damage process, it is common practice to take a representative elementary volume (REV) inside the material that is sufficiently large relative to the micro-fissures and micro-cracks, and sufficiently small relative to the entire material. When geological materials undergo plastic deformation, a dilatancy effect will occur. As the dilatancy behavior is mainly due to the initiation and expansion of microcracks, the microcracks can be considered to be uniformly distributed on the entire material at the REV scale.

In continuum damage mechanics, the elastic modulus of the element is assumed to be degraded gradually as damage progresses. The damage softening of the coal body is due to the volume expansion caused by the development of micro-fractures, and is in line with the damage law of geological materials in the form of an exponential function. The stress–strain curve of each element is considered to be linearly elastic before the given damage threshold is reached. Therefore, combined with previous studies, the following damage evolution equation is proposed [33]:

$$D = 1 - \exp\left(-\left(\frac{\varepsilon^V - \varepsilon_I^V}{F}\right)^m\right) \qquad (1)$$

where ε^V is the volumetric strain; ε_I^V is the volumetric strain threshold; i.e., the damage starts when the volumetric strain reaches this threshold, which reflects a reasonable starting point of the damage of rock [34]; F is the rock strength parameter, reflecting the average strength based on macroscopic statistics; m is a constant, reflecting the concentration degree of the coal strength distribution. In this study, the element becomes damaged when the stress in the element satisfies the strength criterion. The element and its damage are assumed to be isotropic. This model alone can predict the non-linear deformation of a quasi-brittle rock.

As the influence of damage on the strain is reflected in the effective stress, the constitutive relation of rock damage can be established according to the strain equivalence hypothesis of Lemaitre [35]. It can be written as follows:

$$\sigma_{ij} = E_{ijkl}\left(\varepsilon_{ij} - \varepsilon_{ij}^p\right)(1 - D) \qquad (2)$$

where σ_{ij} is the stress; E_{ijkl} is the elastic modulus; ε_{ij} is the overall strain; ε_{ij}^p is the plastic strain.

The failure of a rock mass is mainly in the form of shear and tension. The Mohr–Coulomb criterion is generally adopted for the shear strength of coal bodies with multiple fractures; thus, the basic form of the shear failure criterion can be written as:

$$F_s = \sigma_1 - \sigma_3 N_{\phi_a} + 2c\sqrt{N_{\phi_a}} \qquad (3)$$

$$N_{\phi_a} = \frac{1 + \sin(\phi_a)}{1 - \sin(\phi_a)}$$

The tensile failure criterion is:

$$F_t = \sigma_3 - \sigma^t \qquad (4)$$

where σ_1 and σ_3 are the maximum and minimum principal stresses, respectively, MPa; Φ_a is the angle of friction, °; c is the cohesion, MPa; σ_t is the tensile strength, MPa.

In the plastic theory, a rule to determine the relationship between the components of plastic strain increment—that is, to specify the direction of plastic strain increment—is called the flow rule. When the stress state reaches the yield surface, the plastic strain increment $d_{ij}{}^P$ under the stress state can be determined by the plastic potential surface g. Plastic potential function is a surface in stress space that is perpendicular to the plastic strain increment. Plastic flow is defined by a flow potential that is associated on the cap and non-associated on the failure yield surface and transition yield surfaces. The potential function is described by means of two functions, g_s and g_t, used to define shear plastic flow and tensile plastic flow, respectively. The non-associated flow rule is adopted with a shear plastic potential function defined as follows [36]:

$$g_s = \sigma_1 - \sigma_3 N_{\psi_a}$$

$$N_{\psi_a} = \frac{1 + \sin(\psi_a)}{1 - \sin(\psi_a)} \tag{5}$$

where ψ_a is the dilatancy angle, °. The tensile plastic potential function is:

$$g_t = \sigma_3 \tag{6}$$

Upon the onset of yielding, plastic deformation should conform to the consistency of the flow potential function [37]. According to the theory of plastic increment, the plastic increment can be obtained using the flow rule [37],

$$\Delta \varepsilon^P = \dot{\lambda} \frac{\partial g}{\partial \sigma_{ij}} \tag{7}$$

Plastic strain is updated at each step when the plastic flow occurs. Equation (2) yields the following:

$$\Delta \sigma_{ij} = \left(E_{ijkl} \Delta \varepsilon_{ij} - E_{ijkl} \Delta \varepsilon_{ij}^P \right)(1 - D) \tag{8}$$

Let the initial stress be $\sigma_{ij}{}^0$, stress before plastic modification be $\Delta \sigma_{ij}{}^I$, stress after plastic modification be $\sigma_{ij}{}^N$, and damage increment be ΔD. Assuming that the coal is an isotropic material, Equation (8) leads to:

$$\begin{cases} \sigma_1^N = \left(\Delta \sigma_1^I - \dot{\lambda}_s \left(\lambda (1 - N_\psi) + 2G \right) \right)(1 - D) + \sigma_1^0 (1 - \Delta D) \\ \sigma_2^N = \left(\Delta \sigma_2^I - \dot{\lambda}_s \left(\lambda (1 - N_\psi) \right) \right)(1 - D) + \sigma_2^0 (1 - \Delta D) \\ \sigma_3^N = \left(\Delta \sigma_3^I - \dot{\lambda}_s \left(\lambda (1 - N_\psi) - 2G N_\psi \right) \right)(1 - D) + \sigma_3^0 (1 - \Delta D) \end{cases} \tag{9}$$

The flow constant λ_s is:

$$\dot{\lambda}_s = \frac{F_s \left(\sigma_1^I, \sigma_3^I \right)}{\left(\lambda (1 - N_\psi) + 2G \right) - \left(\lambda (1 - N_\psi) - 2G N_\psi \right) N_\phi} \tag{10}$$

The modified stress under tensile failure is:

$$\begin{cases} \sigma_1^N = \left(\Delta \sigma_1^I - \dot{\lambda}_t \lambda \right)(1 - D) + \sigma_1^0 (1 - \Delta D) \\ \sigma_2^N = \left(\Delta \sigma_2^I - \dot{\lambda}_t \lambda \right)(1 - D) + \sigma_1^0 (1 - \Delta D) \\ \sigma_3^N = \left(\Delta \sigma_3^I - \dot{\lambda}_t (\lambda - 2G) \right)(1 - D) + \sigma_1^0 (1 - \Delta D) \end{cases} \tag{11}$$

The flow constant λ_t is:

$$\dot{\lambda}_t = \frac{F_t \left(\sigma_1^I, \sigma_3^I \right)}{\lambda - 2G} \tag{12}$$

The failure criterion established above can effectively determine the failure type of the element, and the corresponding plastic strain correction can be performed. Meanwhile, the change in the effective stress under the influence of damage is considered to obtain a reasonable stress value. The variables are updated with every iteration. A comparison between the simulated stress–strain curve and experimental data under uniaxial compression has been conducted to validate the proposed model [33].

3. Permeability Model of Mining-Induced Fracture

After coal mining, the overlying strata gradually collapse and form a mining-induced fracture field (Figure 1), included in the goaf. After the overlying coal seam mining, there is fracture development both above and under the caving zone. The fractures are subjected to combined shear/tensile stress [38]. The shear and tensile deformation of fractures result in a dramatic change in the permeability, which is related to the change in the fracture aperture. There are two interactive behaviors, including shear dilation aperture, caused by shear slippage and the normal aperture change due to tensile failure [39].
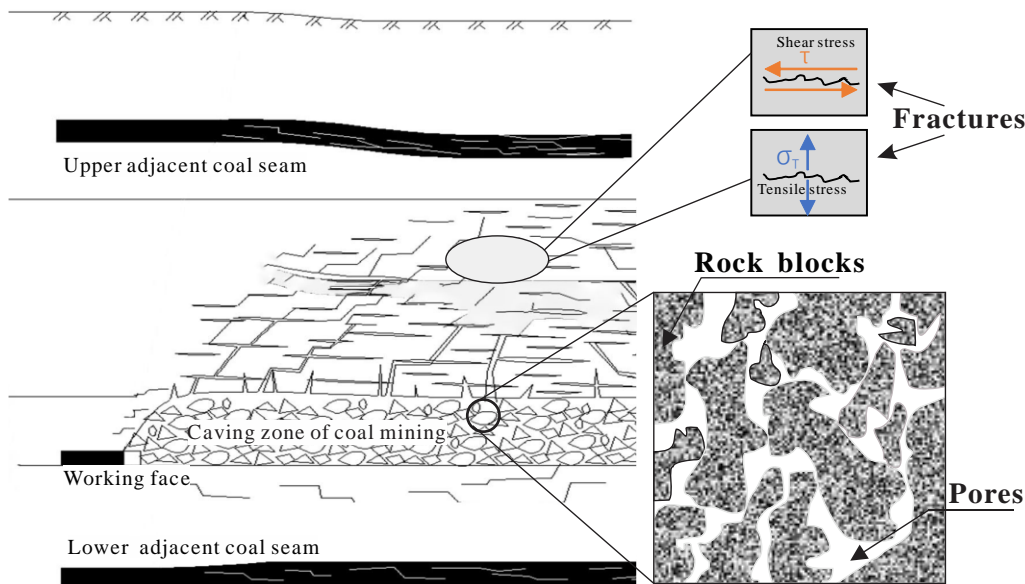

Figure 1. Schematic diagram of the caving zone of coal mining.

Based on the fractal characteristics of fracture surfaces, the permeability model for the fractures subject to shear and tension is given [32,40]:

$$b = b_r + \left(b_f + A(\delta_s)^H \exp\left(-kW_p \right) \right) \exp\left(-\sigma_n C_f \right)$$

$$\frac{k_f}{k_f^0} = \frac{(b)^3}{(b_0)^3} \tag{13}$$

where b is the fracture aperture, b_r is the "hard" part of the fracture aperture or the residual fracture aperture that does not change with stress, b_f is the stress-sensitive part, and C_f is the fracture compressibility. Where δ_n is the normal displacement induced by shear, δs is the shear displacement, H is the Hurst coefficient of fracture surfaces which characterizes the fracture roughness, Wp is the plastic work done by shear on the fracture, A and k are two constants, and k0fi is the initial permeability. This model is based on the two-part Hooke's model (TPHM) proposed by Liu et al. [41]. The permeability model has been validated against experimental data [40]. A comparison between model results and experimental data was performed to validate the proposed model [33]. The complex coupling of damage and shear dilation on gas flow in the process of uniaxial compression has been revealed.

Numerical results show that the accumulation of damaged elements largely controls the failure of rock, and the location of permeability change is highly related to the damage zone.

4. Evolution of Fractures of Close-Distance Coal Seam Group

The subject of this study was working face 28202 in the second mining area of Dongqu Mine, Xishan Coalfield, Shanxi Province, China. The upper part of the coal seam in the mining area is the Lower Permian Shanxi Formation and the lower part is the Upper Carboniferous Taiyuan Formation. The average thickness of the two coal seams is approximately 14.4 m, there are 15 coal layers in total, and the average coal bearing coefficient is approximately 9.1%. Coal seams 2#, 3#, 8#, and 9# are stable and recoverable; coal seams 6# and 7# are relatively stable and mostly recoverable; the other coal seams are unstable and partially recoverable or unrecoverable.

Working face 28202 is located at +860 level in the second mining area of Dongqu Mine, coal seam 8#. The working face elevation is in the range of 882–923 m, the ground elevation is in the range of 1042 m–1215 m, and the thickness of the cover mountain is in the range of 148–293 m. Coal seams 2# and 4# above have been mined instead of coal seam 7#. The interval between coal seams 4# and 8# is in the range of 66–81 m. The working face strike length is 978 m, and the dip length is 206 m. The structure of this working face coal seam is complex, and its occurrence is relatively stable. The thickness of the coal seam 8# is between 2.2 and 3.8 m, with an average thickness of 3.3 m. The coal seam is intercalated with one to three layers of gangue. The dip angle of the coal seam is in the range of 2–8°, with an average dip angle of 5°. The pseudo roof of working face 28202 is not developed, and the direct roof is carboniferous shale with a thickness of 2.04 m, the old roof is limestone with a thickness of 2.55 m, and the coal seam floor is sand shale with a thickness of 6.24 m. Roof strata have a small fluctuation. The spatial position relationship between working face 28202 and other coal seams are: coal seam 2#, with a thickness of 1.78 m, is located in the working face roof with a spacing of 83.35 m; coal seam 4#, with a thickness of 2.97 m, is located in working face 28202 roof, with a spacing of 66 m; coal seam 7#, with a thickness of 0.85 m, is located in the roof of working face 28202, with an interval of 29 m; coal seam 9#, with a thickness of 2.70 m, is located in the bottom plate of working face 28202, with an interval of 8.94 m.

4.1. Simulation Models

The 3DEC three-dimensional discrete element method was used to simulate and analyze the development law and evolution process of the overburden fracture field in the goaf, which can provide guidance for drilling and gas drainage design [42]. Figure 2 shows the numerical geometric model structure with working face 28202 as the prototype.
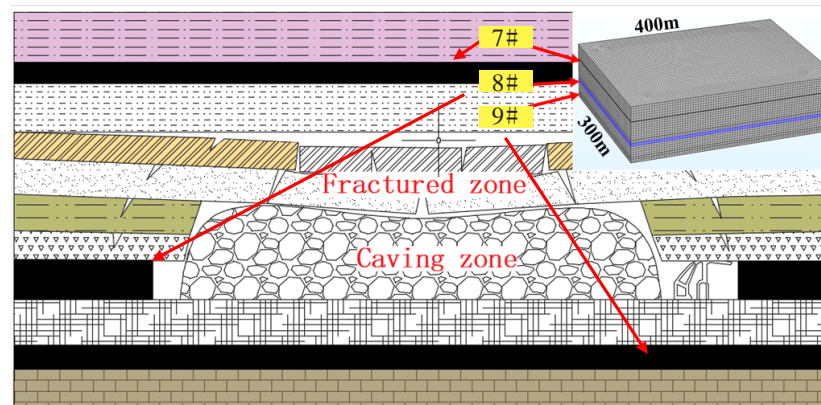

Figure 2. Geometric model of rock strata.

Coal is a sedimentary rock type, which has experienced a long deposition process. Many bedding planes and cleats in the coal mass result in anisotropic mechanical properties. These fractures typically can be divided into two types: face cleat and butt cleat. These two sets of coal cleats are perpendicular or nearly perpendicular to each other and intersect the coal to form an interconnected network throughout a coal-bed. Fractured sedimentary rock also contains two domains, fractures, and an adjoining rock matrix. Overburden movement is associated with the problem of separation fracture, and 3DEC V4.1 software based on the discrete element has a good advantage in simulating discontinuous media. The software represents discontinuous media by discrete blocks, the discontinuities are treated as boundary surfaces between the blocks, and large displacement and rotation of the blocks along the discontinuities are allowed. Individual blocks behave as either rigid or deformable material. Deformable blocks are subdivided into a mesh of finite difference elements, and each element responds according to a prescribed linear or nonlinear stress–strain law. The relative motion of the discontinuities is also governed by linear or nonlinear force-displacement relations for movement in both the normal and shear directions. 3DEC has several built-in material behavior models, for both the intact blocks and the discontinuities, that permit the simulation of response representative of discontinuous geologic, or similar, materials. 3DEC is based on a Lagrangian calculation scheme that is well suited to model the large movements and deformations of a blocky system.

Early distinct element codes assumed that blocks were rigid. However, the importance of including block deformability has become recognized, particularly for stability analyses of underground openings and studies of seismic response of buried structures. The Mohr–Coulomb model was formed based on the maximum shear stress to predict shear damage, and is widely used. However, the Mohr–Coulomb (M–C) strength criterion is a linear criterion, which cannot accurately describe the nonlinear properties of the rock strength under different confining pressures. Therefore, this paper attempts to incorporate the nonlinear response into the M–C strength criterion to overcome the above limitations. The modified Mohr–Coulomb strength criterion and the statistical damage constitutive model were proposed in the simulation. The damage constitutive model was used to characterize coal block damage and deformation, and a code file "Damage_mechanical_model.dll" for the damage model was developed using C++ UDM (User-Defined constitutive Models) subroutine. The Mohr–Coulomb slip model is used for fracture deformation in this paper. The Coulomb slip model requires six parameters: normal and shear stiffness, friction angle, cohesion, tensile strength, and dilation angle. The permeability distribution is calculated based on exported data of shear stress for all joints. The flow diagram of the calculation cycle in 3DEC is shown in Figure 3.

In the 3DEC model, two sets of cleats are defined based on the geological condition in the study area. The mechanical properties of the rock mass and the discontinuities for different lithologies are provided in Table 1. The Mohr–Coulomb failure criterion was adopted to assess fault reactivation or fault slippage. The original cleats are subjected to high shear stress and tensile stress in the fractured zone under the coupling action of the overburden stress and mining-induced stress. This results in significant fracture development in the fractured zone. The horizontal displacement was fixed at the vertical boundary of the model, the vertical displacement was fixed at the bottom boundary, and overburden pressure was applied at the top. Table 1 presents the simulation parameters. The mechanical parameters of the coal were determined from the results of the mechanical test, and the average values of the mechanical parameters of the obtained coal were summarized and used as the parameters of the numerical simulation experiment. Some parameters which were not available during our laboratory tests were collected from documentation provided by the coal mine company.
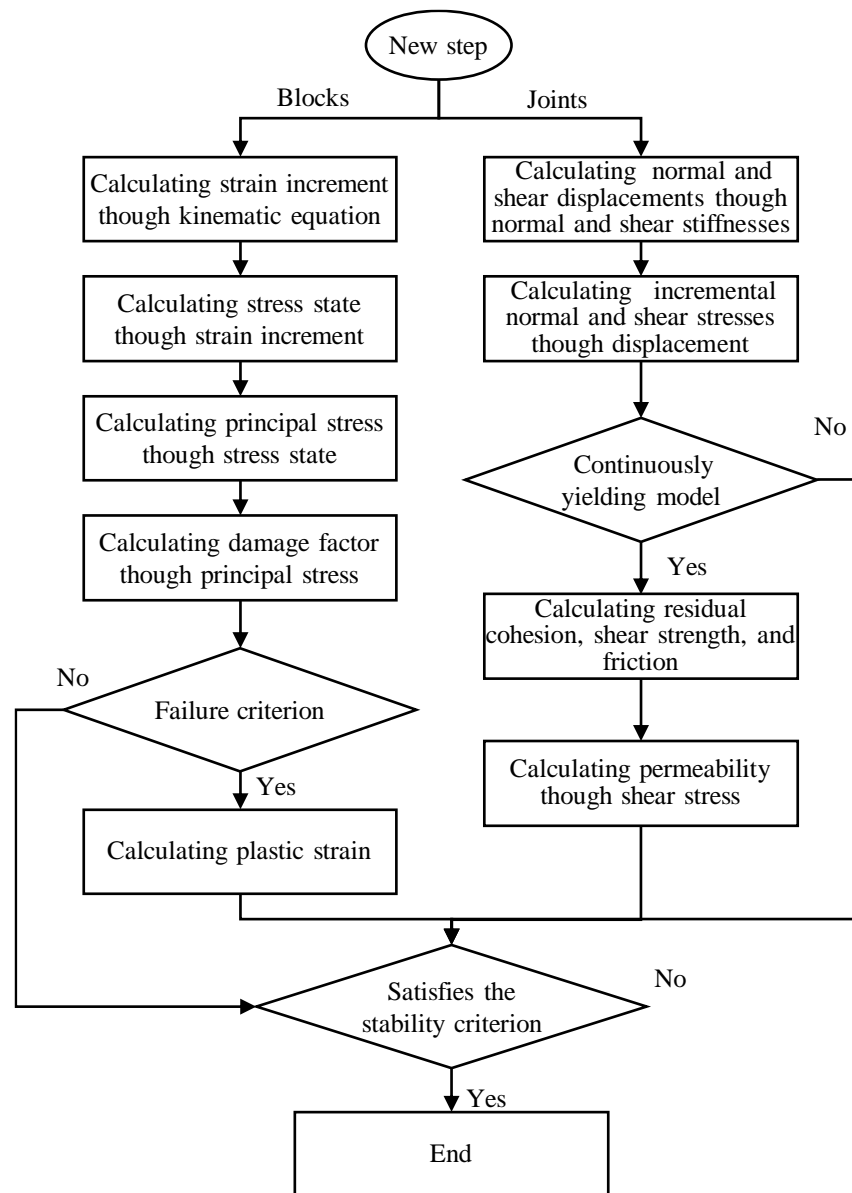
```
                              ┌───────────┐
                              │ New step  │
                              └───────────┘
            Blocks                              Joints
```

Figure 3. Flow diagram of calculation cycle.

Table 1. Parameters for simulation.

Parameters	Values
Volumetric strain threshold of coal, $\varepsilon_I{}^V$	0.01
Constant, m	3
Angle of friction of coal, Φ_a	24°
Tensile strength of coal, σ^t	2.5 MPa
Cohesion of coal, c	1.2 MPa
Young's Modulus of coal, K	2713 MPa
Possion's ratio of coal, ν	0.339
Density of coal, ρ_M	1400 kg/m^3
Fracture aperture, b_0	1×10^{-4} m
Residual fracture aperture, b_r	5×10^{-5} m
Stress-sensitive portion of the fracture aperture, b_f	5×10^{-5} m
Fracture compressibility, C_f	1×10^{-8} Pa^{-1}
Constants, A	0.2 m

Table 1. *Cont.*

Parameters	Values
Constants, k	7×10^{-6} m/N
Hurst coefficient for a fracture surface, H	0.85
Joint normal stiffness of coal	2000 MPa/m
Joint normal stiffness of sandstone	2900 MPa/m
Joint normal stiffness of mudstone	2200 MPa/m
Joint shear stiffness of coal	1900 MPa/m
Joint shear stiffness of sandstone	2500 MPa/m
Joint shear stiffness of mudstone	2000 MPa/m
Tension capacity of coal	0.07 MPa
Tension capacity of sandstone	0.1 MPa
Tension capacity of mudstone	0.09 MPa

The 3DEC V4.1 software was utilized to simulate the distribution characteristics of the fracture network in the overlying mining rock mass, and the evolution law of the permeability in the fracture field was further obtained by applying Equation (13).

In order to select the position of high drainage roadways that applied to prevent and control gas overruns at the working face, simulation results are used to ascertain distribution characteristics of overburdened cracks caused by the mining process of the working face, as shown in Figure 4.
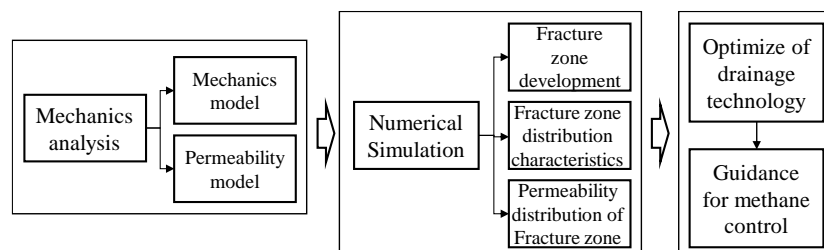
Figure 4. Overview diagram.

4.2. Fracture Evolution of Overlying Strata

In this section, the 3DEC V4.1 software was used to simulate the overlying strata collapse and fracture field development process after mining in coal seam 8#, to obtain the overburden collapse state and the damage degree of the surrounding rock at different times, which were used to calculate the opening value of the fracture. The simulation process was divided into three steps. The first simulation pushed forward to 65 m and then waited for 10 days to obtain the evolution process of the overburden collapse and fracture zone. Thereafter, the simulation pushed forward to 120 m to observe the overburden state changes, and finally pushed forward to 180 m. The overlying strata exhibited a periodic collapse, forming a collapse zone, a fracture zone, and a bending subsidence zone.

Figure 5 shows the distribution of the overburden displacement and fracture opening after 65 m advancement of the working face. In the initial stage, the direct roof bending subsidence was the largest at the center of the goaf, and the subsidence at the mining boundary gradually decreased. As the fracturing of the old roof continued, the overall subsidence in the caved area kept increasing. As shown in Figure 6, the bottom plate also bulges with a displacement of 12 cm. In the initial stage, the distribution of the fractures between rock strata was relatively uniform. In the vertical direction, the fracture aperture is mainly determined by the vertical displacement of the rock stratum. The bending and subsidence of the overburden led to the separation of rock strata and a channel for gas to flow through.
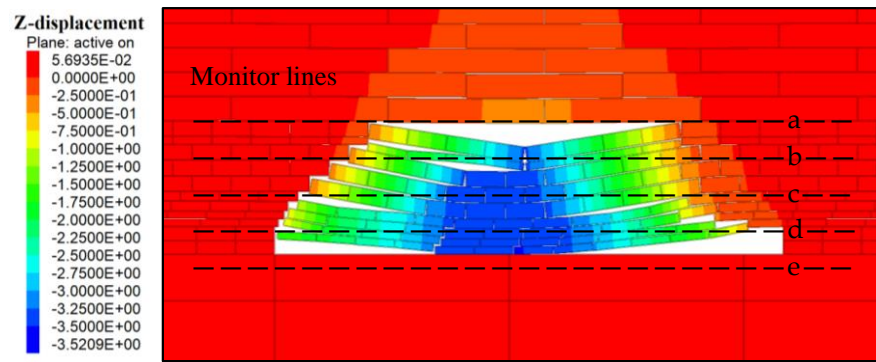
(**a**) Vertical displacement
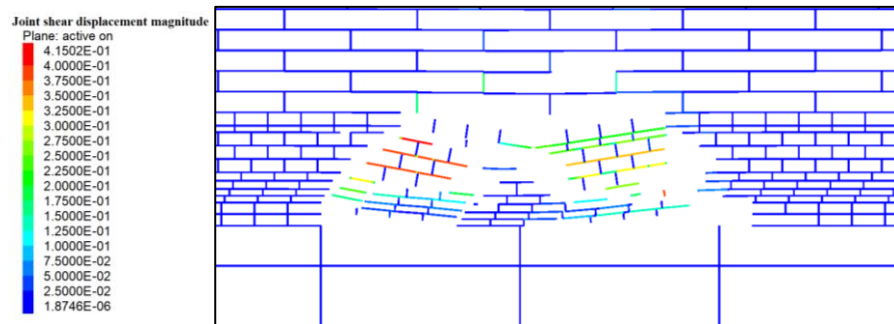
(**b**) Fracture aperture

Figure 5. Distribution of displacement and fracture aperture after working face advanced to 65 m. (Line a, b, c, d, and e are monitor lines).
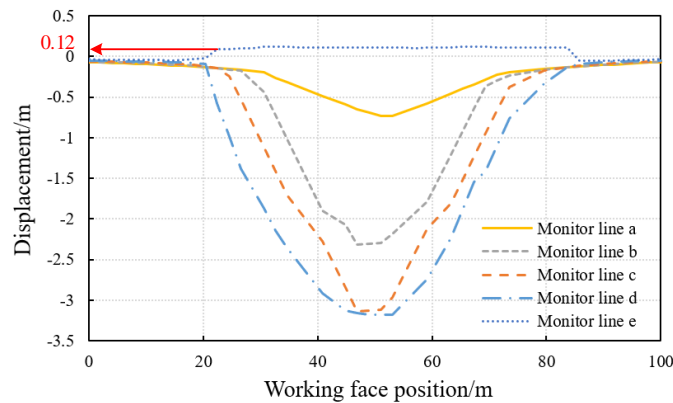

Figure 6. The curves of vertical displacement at different heights of rock strata after working face advanced to 65 m.

When the excavation reached 120 m, a wide range of bending subsidence occurred, leading to periodic pressure variation. From the displacement curves of the rock strata at different positions, as shown in Figures 7 and 8, we find that the roof strata above goaf present overall subsidence before the position of the working face. Due to the cantilever beam support, the amount of subsidence within 10 m behind the working face was small, but the amount of subsidence gradually increased in the area where the overburden was fractured. Meanwhile, the floor continued to heave, and the displacement was 15 cm. As shown in Figure 7b, the fracture opening at the goaf boundary position was large, and the overburden separation at the top increased after 120 m, resulting in an increase in the fracture opening. At the original working face position of 65 m, due to roof collapse, the cracks were compressed in the center but remained open at the 120 m position. The roof

fracture caused the increases in the crack density and aperture in the goaf boundary. At this stage, the gas flow channel was mainly located within 30 m behind the working face.
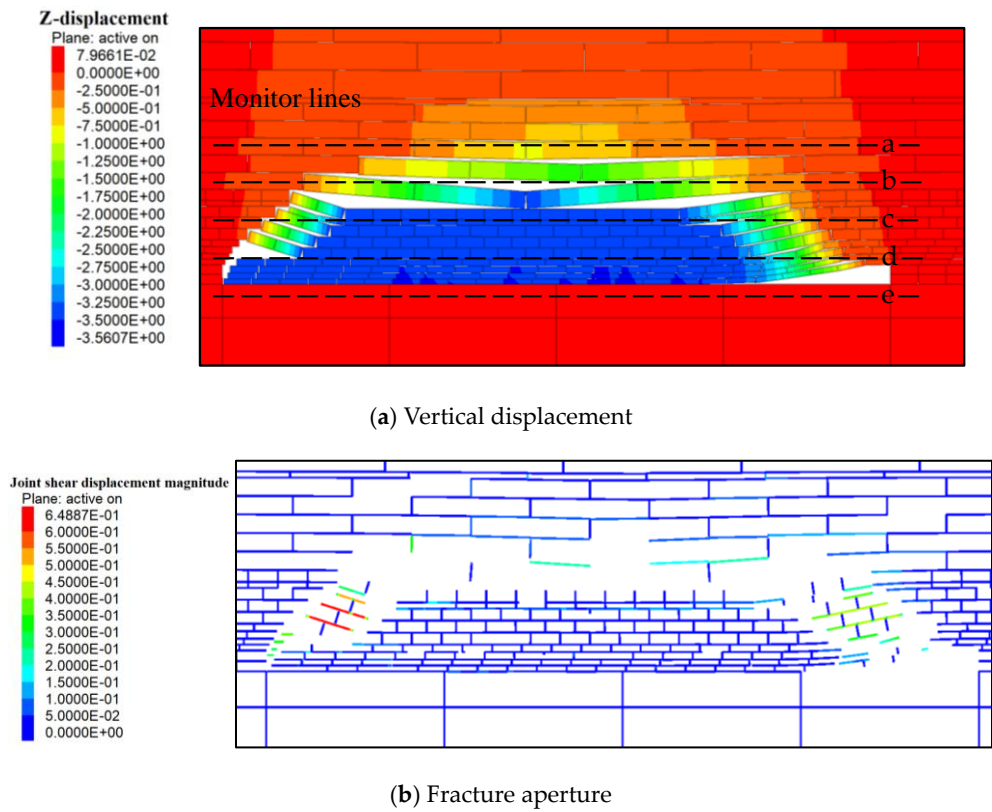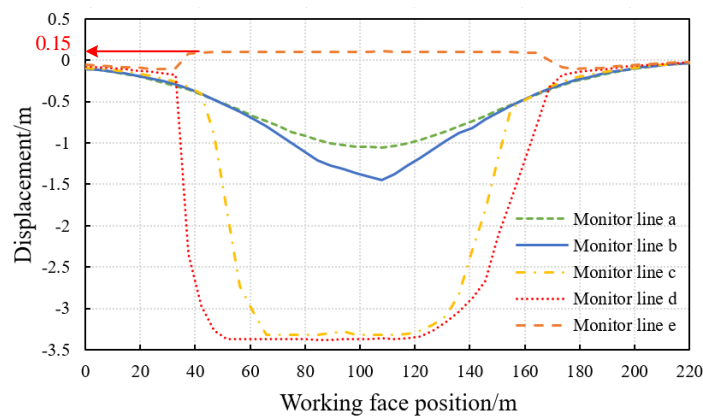

(**a**) Vertical displacement

(**b**) Fracture aperture

Figure 7. Distribution of displacement and fracture aperture after working face advanced to 120 m. (Line a, b, c, d, and e are monitor lines).

Figure 8. The curves of vertical displacement at different heights of rock strata after working face advanced to 120 m.

As the working face continued to advance, the overlying strata collapsed periodically. Behind the new caved strata, the old fractures closed, the collapsed rock mass in the middle of the goaf was compacted, and the collapse swelling rate of the caved strata was reduced. As shown in Figures 9 and 10, when the advance reaches 180 m, the range of collapsed overburden continues to increase, the floor continues to bulge, the vertical displacement is 16 cm, and the bending band extends to a large range. The fracture was well developed. In the goaf boundary region, the fracture opening was large, and the separation layer existing in the bending zone also increased the fracture opening. The rock stratum dislocation at

the goaf boundary location caused a shear deformation of the fracture, resulting in the formation of a gas seepage channel. A shear failure zone surrounding the shearing fracture is gradually developed during shear, in which the failed fractures have greater apertures than the undamaged fractures due to shear-induced dilation.
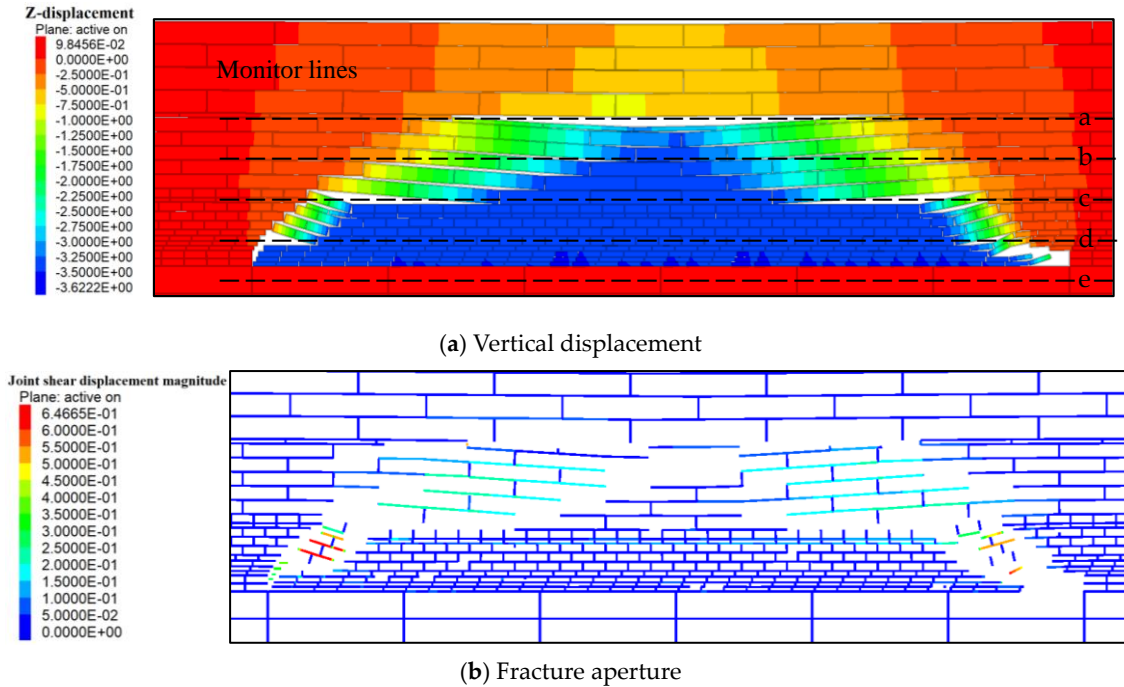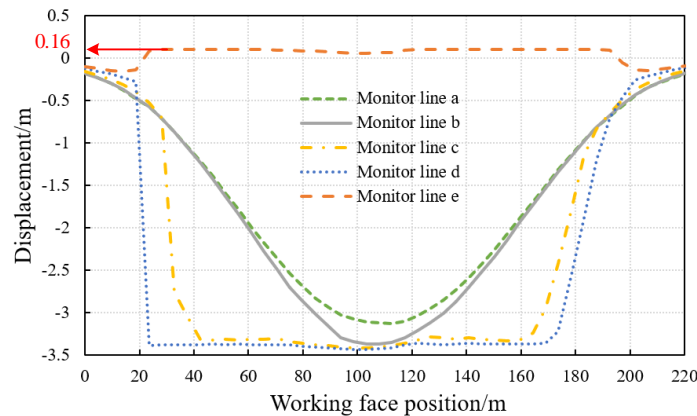

(**a**) Vertical displacement

(**b**) Fracture aperture

Figure 9. Distribution of displacement and fracture aperture after working face advanced to 180 m. (Line a, b, c, d, and e are monitor lines).

Figure 10. The curves of vertical displacement at different heights of rock strata after working face advanced to 180 m.

The numerical simulation results showed that with the advance of the working face, the fracture zone in the goaf evolves temporally and spatially. Hence, the predicted distribution of the fracture zones allows for the estimation of where the gas drainage can be effectively performed. Figure 11 shows the heights of the three typical zones varying with the advancing distance of the working face. The thickness of the three zones at different depths increases with increasing advancing distance. However, the permeability evolution of the three zones depends on the stress states that change with coal mining. This indicates the fracture and permeability evolutions with time and space during the mining of a coal seam.
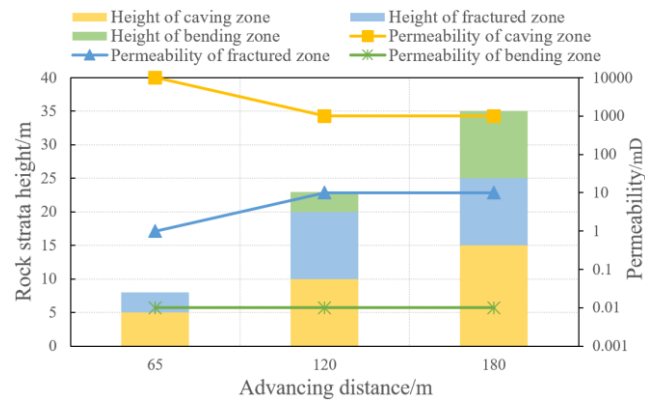
Figure 11. Permeability enhancement versus rock strata height at different distances.

4.3. Stress Relief on Adjacent Coal Seams

Under the condition of close-range coal seam groups, the coal seam above and below a certain range of mining produces fractures due to the stress relief, thus forming a high-permeability area. In a close-distance coal seam group, the adjacent coal seams are under more severe stress relief effects. Figure 12 shows the shear strain distribution in the upper and lower adjacent coal seams during the advance of the working face. As shown, the stress relief laws of mining on the upper and lower adjacent coal seams are different. The stress is gradually relieved in the lower and upper adjacent coal seams. Above the overburden collapse zone, because the tensile strength in the strata was much greater than the strength of the interlayer bedding, the strata bent and sank, leading to a shear deformation between the strata. The coal seams had a lower relative strength and greater shear strain. The adjacent coal seams had a varying shear strain concentration area as the working face advanced. In the upper adjacent coal seam, the shear strain was mainly concentrated above the permanent and moving boundaries, and the concentration area of the shear strain moved continuously with the advance of the working face. However, the lower adjacent coal seam was below the goaf, and the influencing range increased with the advance of the working face.

Due to the dilatancy effect of the mining-induced fractures, the permeability of the fractures increased exponentially during shearing. Figure 13 shows the distribution patterns of the upper and lower adjacent coal seams. In the upper and lower adjacent coal seams, the permeability increased within 40 m of the goaf boundary, and the increase of the permeability became more significant as the working face advanced. When the working face advanced to 65 m, the permeability increased by 4000 times, whereas it increased by 20,000 times when the working face advanced to 180 m. The area where permeability increased was expanded as the working face advanced.
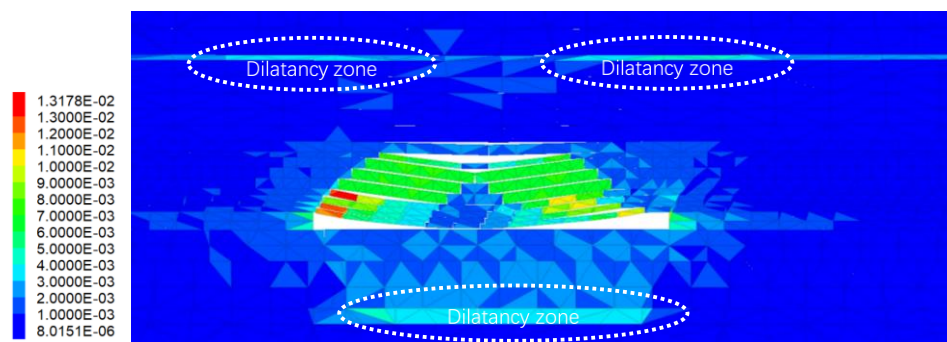
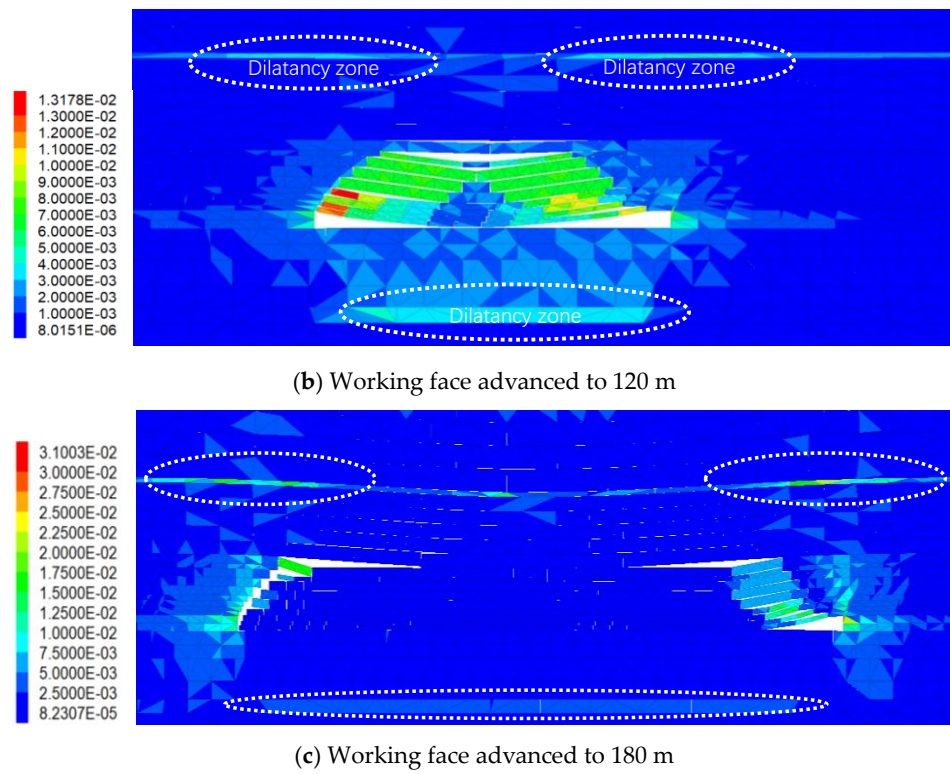(**a**) Working face advanced to 65 m

Figure 12. *Cont.*

(**b**) Working face advanced to 120 m

(**c**) Working face advanced to 180 m

Figure 12. Distribution of shear strain under different advanced distance.

(**a**) Working face advanced to 65 m

(**b**) Working face advanced to 120 m
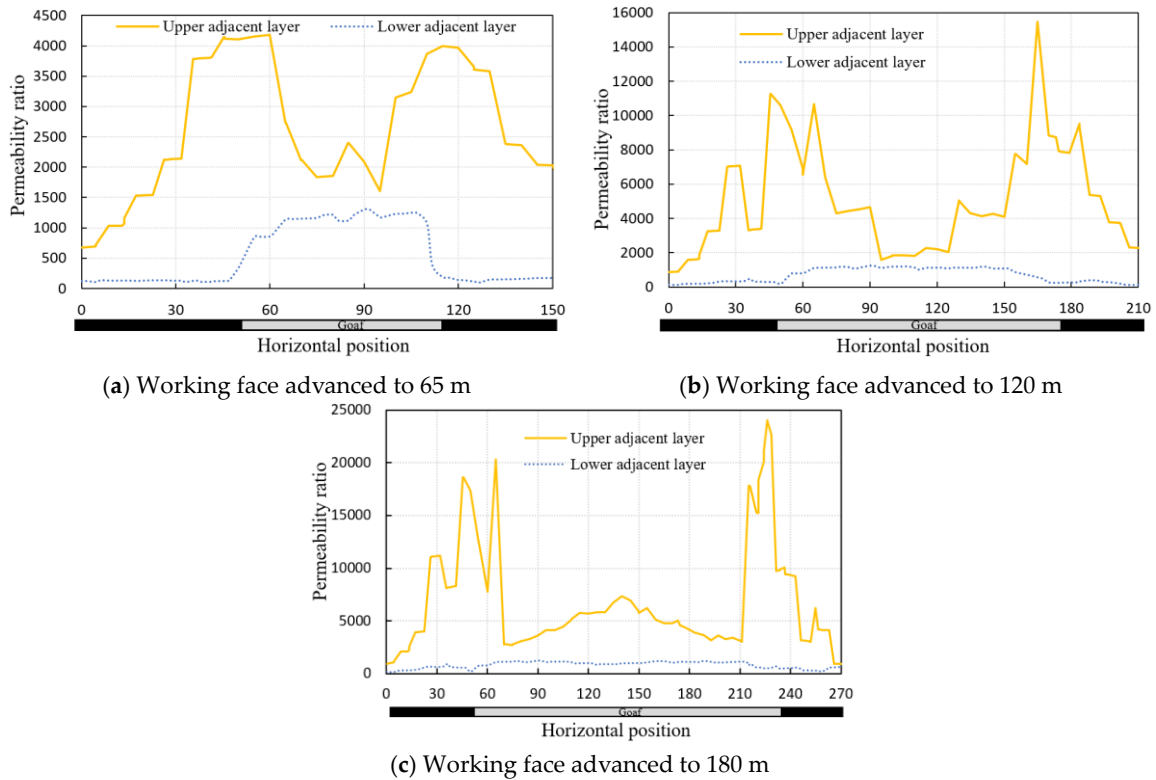

(**c**) Working face advanced to 180 m

Figure 13. Permeability evolution of adjacent coal seam after mining-induced stress relief.

In the lower adjacent coal seam, permeability increased by approximately 1500 times after excavation, but it did not change significantly as the working face advance. Thus, the lower and upper adjacent coal seams were impacted differently by the excavation-induced stress relief in the scenario of close-distance coal seam mining.

5. Discussion

5.1. Design Parameter of High-Level Suction Roadway

Understanding the evolution and distribution of the mining-induced fractures in the overlying strata helps select the position of high drainage roadways. The application of the high suction roadway is to extricate more goaf gas of high concentration and reduce gas emission quantity at the upper corner during mining activities.

Based on a quantitative analysis of the gas source during the mining of coal seam 8#, the gas source in the overlying coal seam accounted for more than 30% of the total gas emission. Therefore, it was necessary to arrange a high-level drainage path to direct the gas flow from the overlying coal seam to the goaf. Combined with the above numerical simulation, the design scheme of the high-level suction roadway is described as follows:

1. From the beginning of the open-off cut, the movement law of the overlying strata in the initial mining stage was considered. Within 65 m of the advancing length along the working face, the high suction roadway should be 25 m in the wrong return air roadway, and the vertical distance from the coal seam increased from 12 to 15 m. After mining was completed, the high-level suction roadway could achieve a good drainage effect in a short time.

2. When the working face length was within the range of 65–110 m, the high-level suction roadway should not be too high and should be arranged in the middle and lower parts of the fracture zone as much as possible. In this case, the vertical distance between the high-level suction roadway and the coal seam increased from 15 to 25 m. The horizontal distance of the inclined working face boundary in the high-level suction roadway was 25 m.

3. When the advancing distance of the working face was within the range of 110–180 m, the high-level suction roadway could be appropriately raised. At this time, the horizontal distance of the inclined working face boundary in the high-level suction roadway was set to 25 m, and the vertical distance between the high-level suction roadway and the coal seam increased from 25 to 35 m.

4. When the advancing distance of the working face was greater than 180 m, the fracture zone was fully developed. At this time, the horizontal distance of the inclined working face boundary in the high-level suction roadway was 25 m, and the vertical distance between the high-level suction roadway and the coal seam was approximately 35 m.

5. The main body of the high-level suction roadway was located in the middle and upper parts of the fracture zone formed by mining in coal seam 8#, and the gas drainage had a wide influence range. The height of the high-level suction roadway was arranged on the basis of different working face mining degrees, in such a way to ensure that the high-level suction roadway was connected to the O-shaped circle formed by working face mining earlier and that the drainage influence range was wide. This measure could effectively cut off the gas influx into the mining space in the entire goaf and surrounding coal-rock mass and allow for effective drainage in the goaf and surrounding coal-rock mass.

5.2. Gas Extraction Efficiency in High–Level Suction Roadway

Based on the design scheme of the high drainage roadway in working face 28202 and the actual geological conditions, a high-level suction roadway was constructed on site to carry out gas drainage in this coal seam, including pre-drainage drilling, low-level suction roadway construction, and drilling in the goaf.

The high-level suction roadway was constructed along the roof of coal seam 7# and ran through the length of the working face strike. The height of the high-level suction roadway has been arranged on the basis of different working face mining degrees. The fault distance between the high-level suction roadway of working face 28202 and its belt routing was in the range of 25–30 m, and the vertical distance between the roadway and coal seam 8# was approximately in the range of 24–45 m. When the open-off cut was 210 m away from working face 28202, the vertical distance between the high-level suction drainage roadway

and coal seam 8# was in the range of 24–40 m. When the open-off cut was 520 m away from working face 28202, the vertical distance between the high-level drainage roadway and coal seam 8# varied in the range of 40–45 m. Thereafter, the vertical distance between the high-level suction drainage roadway and coal seam 8# was in the range of 24–40 m. Figure 14 shows the specific locations of the high-level suction drainage roadway and a working face.
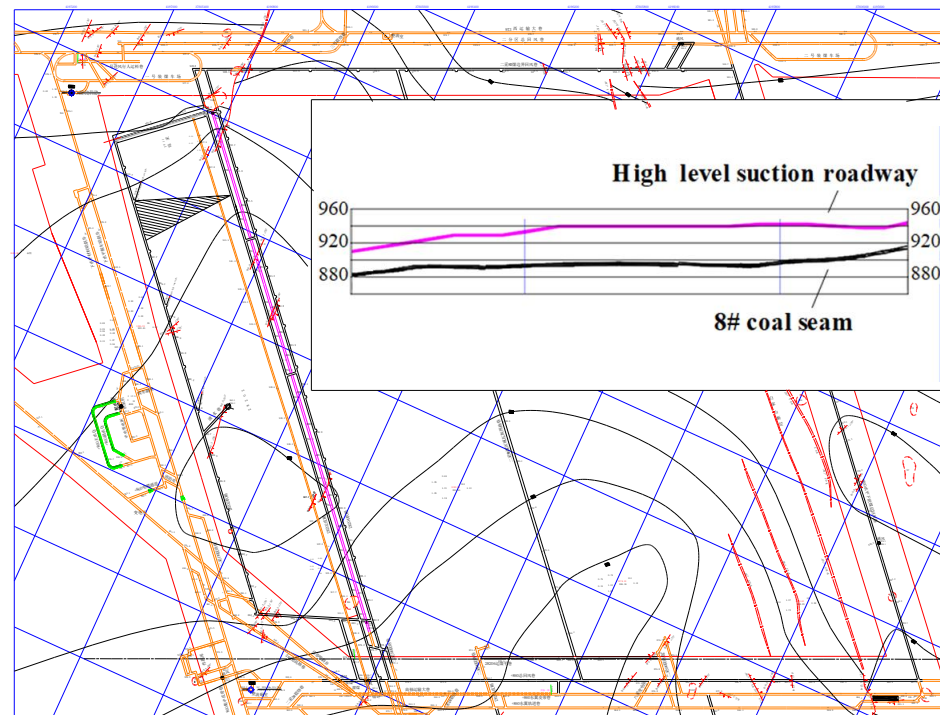

Figure 14. Cross-section map of high-level suction drainage roadway. (Magenta line is high level suction roadway, and black line is coal seam).

Figures 15 and 16 show the changes in the gas concentration and drainage volume in the high-level suction roadway of working face 28202. During the initial production period of the working face, the surrounding rock above the goaf had not completely collapsed, and the gas in the goaf had not entered the high-level suction roadway, because of which the gas concentration in the high-level suction roadway was below 5%, and the absolute gas emission was less than 10 m^3/min. After advancing to 114 m, with the bending and fracture of the goaf overlying strata, a fracture channel was formed between the high-level suction roadway and goaf in the upper fracture zone of the goaf, gradually increasing the gas concentration in the roadway. This zone is more permeable than other areas, which is responsible for the enhancement of permeability. As the working face continued to advance to a range of 300–500 m, the surrounding rock at the upper part of the working face periodically collapsed, resulting in a gradual increase in the gas concentration in the high-level suction roadway during this period, while the absolute gas emission was stable at approximately 9%. When the advancing distance of the working face was more than 600 m, the absolute emission amount of the gas drainage from the high-level suction roadway decreased slightly with the decrease in the air distribution volume.

The advancing distance of working face 28202 was 776 m for five months, during which the peak gas drainage flow was 25.91 m^3/min, and the minimum gas drainage flow was 7.3 m^3/min, resulting in an average gas drainage flow of 15.62 m^3/min in the high-level suction roadway, 56.1% of the average gas drainage flow (27.86 m^3/min). Additionally, the average absolute gas emission in the working face was 39.32 m^3/min, with the average gas

emission of the air exhaust accounting for 39.7%. The above results show that the high-level suction roadway had a remarkable effect on the gas drainage.
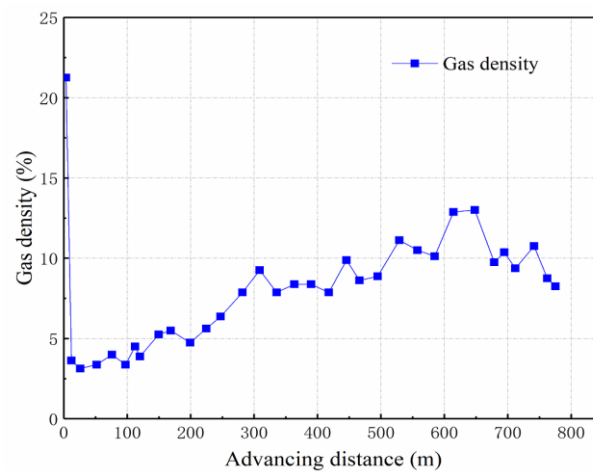

Figure 15. The concentration of gas extraction in high-level suction drainage roadway.
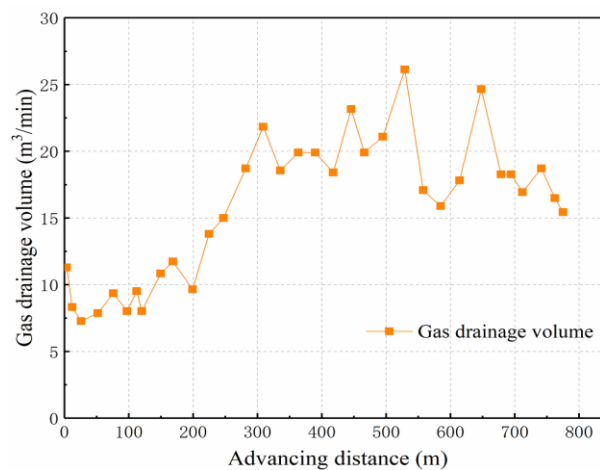

Figure 16. The quantity of gas extraction in high-level suction drainage roadway.

Figure 17 shows the ratios of the gas emission by air exhaust, high-level suction drainage roadway, low-level suction drainage roadway, drainage in this coal seam, buried pipe drainage in the upper corner, and buried pipe drainage in the goaf. As observed, when working face 28202 was in the initial stage of mining (less than 120 m), the contact channel between the high-level suction drainage roadway and the working face goaf was not well ventilated, and the gas was mainly drained by air exhaust on site while the gas drainage of the high-level suction drainage roadway accounted for approximately 20% of the total gas emission of the working face. However, when the working face reached full mining along the strike, the contact channel between the high-level suction roadway and the working face goaf was well ventilated, as discussed above, and the gas drainage of the high-level suction drainage roadway reached 40%–50% of the total gas emission of the working face in the normal production period. Based on the evolution and distribution law of the overlying strata mining-induced fracture field under mining conditions, after the arrangement of the high-level suction drainage roadway, the drainage effect was significant, and the gas influx into the mining space of the goaf and surrounding coal-rock mass was effectively cut off. This helped maintain a high and stable yield of the working face while ensuring safety.
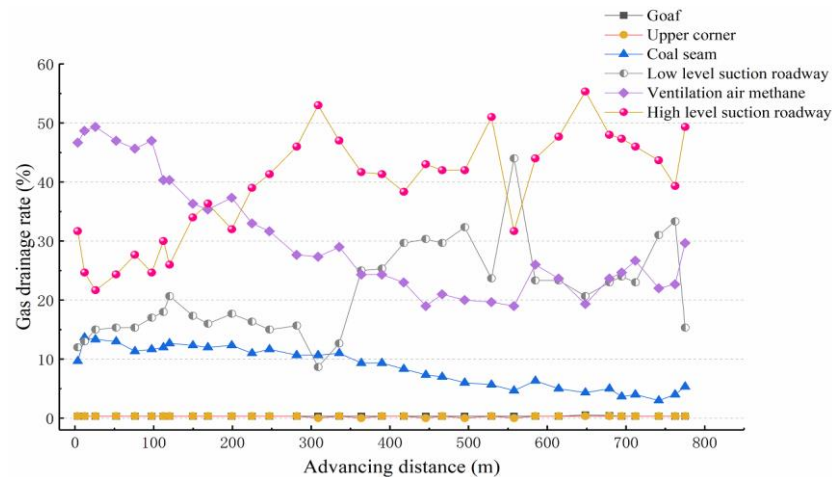
Figure 17. The quantity of gas extraction at different locations.

6. Conclusions

In this study, the evolution of the overburden fracture zone in the process of mining in close-distance coal seam groups were investigated using 3DEC V4.1 numerical simulation software. When the working face advanced from 65 m to 180 m, fractures were mainly concentrated in the lower part of the fracture zone located 20 m above the goaf, and the fracture square above the permanent boundary was fully developed. As the working face advanced, the overburden collapse area continued to increase, the overlying strata increased substantially, the bending zone extended to a significant extent, and the upper coal seam was completed in the bending zone, which significantly improved the permeability of the coal seam.

Mining-induced stress relief had different impacts in the lower and upper adjacent coal seams. The concentration area of the shear strain in the adjacent coal seams varied with the advance of the working face. The permeability enhancement area of the upper adjacent coal seam was located within 40 m of the goaf boundary, and the permeability enhancement effect was significant as the working face continued to advance. The permeability enhancement area of the lower adjacent coal seam was consistent with the position of the goaf, which increased with the completed distance of the working face. The permeability enhancement effect of mining in the lower adjacent coal seam was unaffected by the advancing distance of the working face.

With the continuous advancement of the working face, the influencing height of mining gradually increased, and the permeability of the central goaf decreased due to overburden collapse and extrusion. The goaf boundary extended and was most significant at the end of the working face. It indicates that shear dilation-induced permeability enhancement is the main controlling factor compared with compaction of surrounding pressure. Additionally, based on the simulation results, a high-level suction drainage roadway was constructed, and an excellent drainage effect was achieved, further ensuring the safe and efficient production of the working face.

Conflicts of Interest: The authors declare no conflicts of interest.

References

1. Fan, C.J.; Yang, L.; Wang, G.; Huang, Q.J.; Fu, X.; Wen, H.J. Investigation on coal skeleton deformation in co2 injection enhanced CH4 drainage from underground coal seam. *Front. Earth Sci.* **2021**, *9*, 766011. [CrossRef]
2. Cheng, Y.P.; Yu, Q.X.; Yuan, L.; Li, P.; Liu, Y.Q.; Tong, Y.F. Experimental research of safe and high-efficient exploitation of coal and pressure relief gas in long distance. *J. China Uni. Min. Technol.* **2004**, *2*, 8–12.
3. Xu, D.L.; Wu R l Wang, J.L.; Meng, L.; Zhang, Y.A.; Sun, X.Q.; Qian, Y.J. Test and application of coal seepage characteristics under the condition of ming. *Coal Mine Saf.* **2017**, *48*, 5–8.
4. Xu, J.L.; Qian, M.G.; Jin, H.W. Study on "coal and coal-bed methane simultaneous extraction" technique on the basis of strata movement. *J. Coal* **2004**, *2*, 129–132.
5. Cheng, Y.P.; Fu, G.H.; Yu, Q.X. Development of gas extraction technology in coal mines of China. *J. Min. Saf. Eng.* **2009**, *26*, 127–139.
6. Cao, J.; Li, W.P. Numerical simulation of gas migration into mining-induced fracture network in the goaf. *Int. J. Min. Sci. Technol.* **2017**, *27*, 681–685. [CrossRef]
7. Hu, B.L.; Chen, G.; Zhang, Y.; Yao, J.B. Analysis on mining-induced crack development features of seam with medium thick magmatic rock roof. *Coal Sci. Technol.* **2011**, *39*, 17–20.
8. Lin, H.F.; Li, S.G.; Cheng, L.H.; Wang, H.S. Experimental analysis of dynamic evolution model of mining-induced fissure zone in overlying strata. *J. Min. Saf. Eng.* **2011**, *28*, 298–303.
9. Zhang, X.B.; Zhang, Y.; Liu, C.A.; Liu, K.M.; Li, C.Y.; Wang, Z.F. Design on borehole drilling site for mine gas drainage based on gas migration features in goaf. *Coal Sci. Technol.* **2012**, *40*, 56–61.
10. Cao, W.Z.; Lei, Q.H.; Cai, W. Stress-dependent deformation and permeability of a fractured coal subject to excavation-related loading paths. *Rock Mech. Rock Eng.* **2021**, *54*, 4299–4320. [CrossRef]
11. Liu, T.; Lin, B.Q.; Fu, X.H.; Liu, A. Mechanical criterion for coal and gas outburst: A perspective from multiphysics coupling. *Int. J. Coal Sci. Technol.* **2021**, *8*, 1423–1435. [CrossRef]
12. Fan, C.J.; Wen, H.J.; Li, S.; Bai, G.; Zhou, L.J. Coal seam gas extraction by integrated drillings and punchings from floor roadway considering hydraulic-mechanical coupling effect. *Geofluids* **2022**, 5198227. [CrossRef]
13. Lin, H.F.; Li, S.G.; Zhao, P.X.; Xiao, P.; Pan, H.Y.; Liu, C. Research progress on pressure released gas drainage technology of mining cracking zone in overburden strata of coal mine in China. *Coal Sci. Technol.* **2018**, *46*, 28–35.
14. Miao, X.X.; Qian, M.G. Research on green mining of coal resources in China: Current status and future prospects. *J. Min. Saf. Eng.* **2009**, *26*, 1–14.
15. Yuan, L.; Guo, H.; Shen, B.T.; Qu, Q.D.; Xue, J.H. Circular overlying zone at longwall panel for efficient methane capture of multiple coal seams with low permeability. *J. Coal* **2011**, *36*, 357–365.
16. Qian, M.G.; Xu, J.L. Study on O-ring characteristics of mining-induced fracture distribution in overburden. *J. Coal* **1998**, *5*, 20–23.
17. Xu, J.L.; Qian, M.G. Study and application of mining-induced fracture distribution in green mining. *J. China Uni. Min. Technol.* **2004**, *2*, 17–20+25.
18. Bai, M.; Elsworth, D. Some aspects of mining under aquifers in China. *Min. Sci. Technol.* **1990**, *10*, 81–91. [CrossRef]
19. Karmis, M.; Triplett, T.; Haycocks, C.; Goodman, G. Mining Subsidence and Its Prediction in The Appalachian Coalfield. In Proceedings of the ARMA US Rock Mechanics/Geomechanics Symposium, College Station, TX, USA, 20–23 June 1983.
20. Palchik, V. Influence of physical characteristics of weak rock mass on height of caved zone over abandoned subsurface coal mines. *Environ. Geol.* **2002**, *42*, 92–101. [CrossRef]
21. Huang, Z.A.; Zhang, Y.H.; Li, S.B.; Ni, W. Application of FLAC in determining the upper and low boundary of the fracturing zone in Shaqu coal mine. *Min. Res. Dev.* **2006**, *1*, 20–21+43.
22. Yang, K.; Xie, G.X. Caving thickness effects on distribution and evolution characteristics of mining induced fracture. *J. Coal* **2008**, *10*, 1092–1096.
23. Li, S.G.; Shi, P.W.; Qian, M.G. Study on dynamic distribution characteristics of mining-induced fractures in overburden ellipsometry zone. *Mine Press. Roof Manag.* **1999**, *Z1*, 44–46.
24. Zhang, Y.J.; Zhang, H.X.; Chen, P.P. Visual exploration of fissure field of overburden and rock. *J. Coal* **2008**, *11*, 1216–1219.
25. Cheng, M.; Fu, X.H.; Kang, J.Q.; Tian, Z.B.; Shen, Y.Y. Experimental Study on the Change of the Pore-Fracture Structure in Mining-Disturbed Coal-Series Strata: An Implication for CBM Development in Abandoned Mines. *Energy Fuels* **2021**, *35*, 1208–1218. [CrossRef]
26. Tu, M.; Liu, Z.G. Research on cracking variation of separated strata in roof of fully mechanized caving mining face. *Coal Sci. Technol.* **2004**, *4*, 44–47.
27. Karacan C, Ö.; Esterhuizen, G.S.; Schatzel, S.J.; Diamond, W.P. Reservoir simulation-based modeling for characterizing longwall methane emissions and gob gas venthole production. *Int. J. Coal Geol.* **2006**, *71*, 225–245. [CrossRef]

28. Lunarzewski, L.L.W. Gas emission prediction and recovery in underground coal mines. *Int. J. Coal Geol.* **1998**, *35*, 117–145. [CrossRef]

29. Yu, Q.X.; Cheng, Y.P.; Jiang, C.L.; Zhou, S.N. Principles and applications of exploitation of coal and pressure relief gas in thick and high-gas seams. *J. China Uni. Min. Technol.* **2004**, *2*, 3–7.

30. Cheng, Y.P.; Yu, Q.X. Safe and efficient co-mining system of coal and gas in coal seam group and application. *J. China Uni. Min. Technol.* **2004**, *2*, 3–7.

31. Zhao, W.; Wang, K.; Zhang, R.; Dong, H.Z.; Lou, Z.; An, F.H. Influence of combination forms of intact sub-layer and tectonically deformed sub-layer of coal on the gas drainage performance of boreholes: A numerical study. *Int. J. Coal Sci. Technol.* **2020**, *7*, 571–580. [CrossRef]

32. Wei, M.Y.; Liu, J.S.; Feng, X.T.; Wang, C.G.; Fang, K.; Zhou, F.B.; Zhang, S.W.; Xia, T.Q. Quantitative study on coal permeability evolution with consideration of shear dilation. *J. Nat. Gas Sci. Eng.* **2016**, *36*, 1199–1207. [CrossRef]

33. Wei, M.Y.; Wang, C.G.; Cui, G.L.; Tan, Y.L.; Zhang, S.W. Influence of damage and dilatancy on permeability evolution of fractured coal. *Rock Soil Mech.* **2016**, *37*, 574–582.

34. Cao, W.G.; Zhao, H.; Zhang, L.; Zhang, Y.J. Statistical softening constitutive model of rock damage considering the influence of damage threshold and its parameter determination method. *J. Rock Mech. Eng.* **2008**, *6*, 1148–1154.

35. Lemaitre, J. A continuous damage mechanics model for ductile fracture. *J. Eng. Mater. Technol.* **1985**, *107*, 83–88. [CrossRef]

36. Itasca Consulting Group, Inc. *FLAC3D User Manuals, Version 2.1*; Itasca Consulting Group, Inc.: Minneapolis, MN, USA, 2002.

37. Desai, C.S.; Siriwardane, H.J. *Constitutive Laws for Engineering Materials with Emphasis on Geological Materials*; Prentice-Hall: Upper Saddle River, NJ, USA, 1984.

38. Li, H.Z.; Huang, B.X.; Cheng, Q.Y.; Zhao, X.L.; Chen, B.; Zhao, L. Mechanism of Single Proppant Pressure Embedded in Coal Seam Fracture. *Energy Fuels* **2021**, *35*, 7756–7767. [CrossRef]

39. Hossain, M.M.; Rahman, M.K.; Rahman, S.S. A shear dilation stimulation model for production enhancement from naturally fractured reservoirs. *Spe J.* **2002**, *7*, 183–195. [CrossRef]

40. Wei, M.Y.; Liu, H.H.; Li, L.C. A fractal-based model for fracture deformation under shearing and compression. *Rock Mech. Rock Eng.* **2013**, *46*, 1539–1549. [CrossRef]

41. Liu, H.H.; Wei, M.Y.; Jonny, R. On the normal-stress dependence of fracture hydraulic properties including two-phase flow properties. *Hydrogeol. J.* **2013**, *21*, 371–382. [CrossRef]

42. Itasca Consulting Group, Inc. *Online Contents for 3 Dimensional Distinct Element Code (3DEC Version 5.0)*; Itasca Consulting Group, Inc.: Minneapolis, MN, USA, 2013.